Eur. J. Mech. B - Fluids 19 (2000) 695–706

S0997-7546(00)00130-8/FLA

Transition studies on an elliptic cone in Mach 8 flow using Filtered Rayleigh Scattering

Mark Huntley *, Alexander Smits

Gas Dynamics Laboratory, Princeton University, Princeton, NJ 08544, USA

(Received 7 April 1999; revised 3 April 2000; accepted 4 April 2000)

Abstract – Boundary layer transition on a sharp-nosed elliptic cone in a Mach 8 flow was experimentally investigated using CO_2-enhanced Filtered Rayleigh Scattering. The 4 : 1 elliptic cone was tested at Reynolds numbers ranging from 0.44×10^6 to 3.5×10^6, based on free stream conditions and streamwise distance measured from the cone tip. Boundary layers ranging from fully laminar to late-transitional in character were imaged using single-shot streamwise, spanwise and planform laser orientations. Images taken of the early stages of transition reveal for the first time that transition begins with the emergence of small-scale structures near the centerline axis of the cone (minor axis), rather than in the outboard cross-flow region. The three-dimensional character of these structures is further explored by simultaneously imaging the planform and spanwise planes. © 2000 Éditions scientifiques et médicales Elsevier SAS

experimental / hypersonic / transition / cone / Rayleigh scattering

1. Introduction

Many aspects of the transition process from laminar to turbulent flow are poorly understood. This is especially true in the hypersonic regime where the experimental database is very small and restricted almost entirely to two-dimensional and axisymmetric flow fields. For these flows computational [1] and experimental [2] results have shown that two-dimensional Mack modes dominate the transition process above Mach 4. Realistic hypersonic lifting bodies, however, possess regions of three-dimensional flow which can drastically alter the transition behavior of the boundary layer. Any three-dimensionality inevitably produces spanwise pressure gradients. These gradients induce crossflow, where the flow direction of the interior of the boundary layer is no longer co-planar with the edge velocity vector. The low-momentum boundary layer fluid near the surface is deflected more than the fluid near the edge of the boundary layer. Crossflow vortices may be established which under some circumstances may dominate the transition process. PSE stability analysis on a 4 : 1 elliptic cone by Huang et al. [3] predicted that transition would occur due to an unstable stationary crossflow vortex at Re_x values as low as 1.3×10^5. Stetson et al. [4] used hot-wire probes to show that crossflow on axisymmetric cones at angle of attack significantly affected transition, but only investigated the leeward and windward rays where the spanwise pressure gradients and associated crossflow were zero. More recent experiments by Poggie and Kimmel [5], also using hot-wires, examined the stability characteristics on a 2 : 1 elliptic cone, but could not conclusively determine the existence of crossflow vortices.

The hot-wire studies provide very limited information on the spatial character of the transition process. Flow visualization can add a great deal of insight into these complex geometries, but for flows above Mach 3, techniques have been restricted primarily to schlieren, shadowgraph and oil flow. The recent efforts of the Gas Dynamics Lab and the Applied Physics Group at Princeton University have led to the application of new laser

* Correspondence and reprints; e-mail: huntley@princeton.edu

diagnostics to hypersonic flow, and the visualization results have provided new insights into the behavior of high-speed flows, as reported here.

2. Experiment

Tests were carried out in the Princeton Mach 8 Facility which is a blowdown tunnel with 0.23 meter axisymmetric test section. The Mach number is 8.0 ± 0.15 over a range of freestream unit Reynolds numbers from 2.0×10^6 to 21×10^6. Stagnation pressure can be varied from 1.0 to 10.3 MPa with stagnation temperatures up to 870 K. The test section has rectangular offset window cavities giving optical access from four sides. Models are mounted rigidly to the tunnel wall through the window cavities which requires the tunnel to be started with the model in place. A detailed description of this facility was given by Baumgartner [6].

In order to extend the experimental data base to three-dimensional configurations, an elliptic cone with 4 : 1 cross section is studied. The model measures 0.242 m with 17.5 degree half-angle on the major axis and was manufactured to match the computations of Huang et al. [3].

Experiments were conducted at a Mach number of 8.0 ± 0.15 with average stagnation temperatures of 783 ± 25 K. Run times were typically about two minutes. The heat energy was stored in 85 m of stainless steel piping which is coiled into 19 turns. The coil was electrically heated to the desired stagnation temperature before the run. For these experiments, the tunnel and model were started moderately cold ($\sim$400 K surface temperature) which resulted in roughly a ± 25 K deviation in stagnation temperature during the run and less than 30 K increase in the surface temperature of the model. Therefore, the cold wall condition produced ratios of T_w/T_o ranging from 0.50 to 0.56 throughout the course of a typical two-minute run. For these experiments, the freestream unit Reynolds number ranged from 2.0×10^6 to 15.9×10^6 by varying stagnation pressures from 0.93 ± 0.02 to 8.17 ± 0.07 MPa.

The experiment used carbon dioxide enhanced Filtered Rayleigh Scattering (FRS) for imaging the freestream flow and the boundary layer [7]. Carbon dioxide is injected upstream of the heater coil assembly in quantities ranging from 1–4% of the total tunnel mass flux. According to our current understanding of the technique, the structure of the boundary layer is imaged by the interface between the cold freestream and the hot boundary layer fluid. As the fluid containing condensed CO_2 becomes turbulent by entrainment into the boundary layer, the temperature rises above the sublimation value and the condensate disappears. The boundary layer is therefore imaged as a region of low intensity Rayleigh signal, bounded by bright freestream regions [7]. Comparisons have been made between the imaged interface and pitot surveys of the laminar centerline boundary layer on the cone. The results show that the height of the interface is within 10% of the measured boundary layer thickness. For supersonic turbulent boundary layers, it has been shown that the technique accurately represents the instantaneous large-scale motions in the middle and outer regions of the boundary layer [8].

A narrow linewidth, injection locked, frequency-doubled Nd:YAG laser is used as the scattering source for the Rayleigh imaging. The laser has a 10 Hz repetition rate with a pulse width of 10 ns. Energy output to the test section was $\sim$35 mJ per pulse at 532 nm. The beam was shaped using a positive and negative cylindrical lens pair which produced a uniform focused sheet approximately 50 mm $\times$ 100 μm. The laser output was tuned to overlap a strong spectral absorption line in iodine vapor. A molecular iodine filter was placed in front of the camera so that stray scattering from the model surface was absorbed. The Rayleigh scattering signal from the moving flow was then Doppler shifted outside the absorption band of the filter so that it could be observed by the camera.

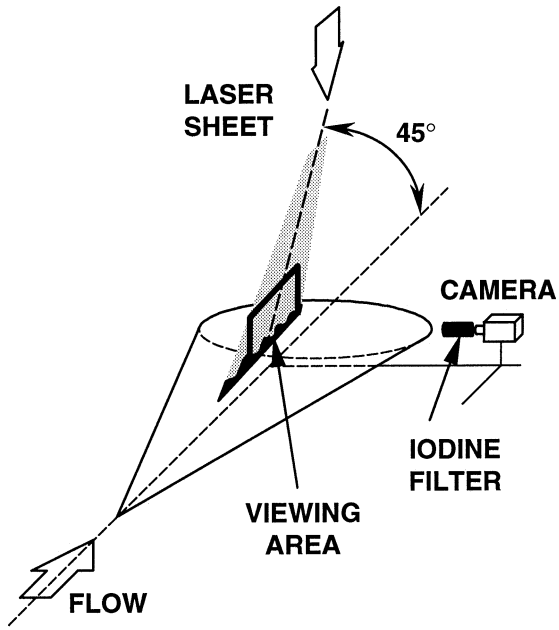

Figure 1. Sheet orientation for streamwise imaging along 4 : 1 model. Laser sheet aligned with centerline of the cone. Field of view was 7 cm in length, centered about the position 20 cm from the nose.

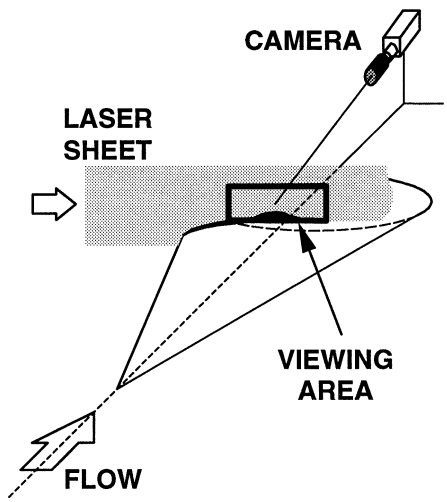

Figure 2. Sheet orientation for spanwise imaging along 4 : 1 model. Laser sheet aligned perpendicular to the flow axis, 21 cm from the nose of the model.

Images of the boundary layer along the model were obtained with streamwise (*figure 1*) and spanwise (*figure 2*) laser sheet orientations. Imaging was accomplished using a double-intensified CID camera with a 100 mm long and 50 mm diameter iodine vapor cell placed in front of the camera lens. For the streamwise view, the camera/filter system was placed orthogonal to the laser sheet with field of view of ∼50 mm along the centerline of the cone. For the spanwise field of view, the camera line of sight was placed at approximately a 30 degree angle with respect to the axis of the tunnel. The camera itself was about 0.75 m downstream of the model looking forward in order to image the plane perpendicular to the flow axis.

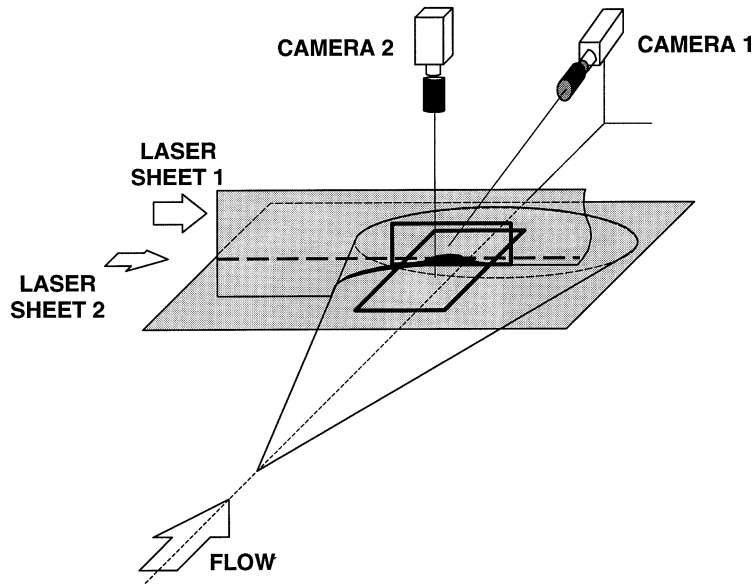

Figure 3. Sheet orientation for simultaneous imaging of spanwise and planform planes. Dashed line represents the intersection of the two image planes.

By splitting a high energy (∼80 mJ) laser pulse into two sheets, simultaneous imaging of the spanwise and planform planes was possible (*figure 3*). The planform plane is defined as the slice across the top centerline (minor axis) of the cone. The laser sheet was expanded in a plane parallel to the centerline ray of the model so that the distance from the sheet to the model surface along the centerline was constant.

The two laser sheets were positioned to overlap at a line approximately 21 cm from the nose of the model. The height of the planform sheet above the model centerline could be adjusted from zero to 6 mm above the surface. Since the imaging planes were nearly perpendicular and Rayleigh scattering is an elastic collision process, the light polarization was rotated to minimize the unwanted signal from the secondary plane, while maximizing the scattering signal to illuminate the desired cross-section of the boundary layer. In this way, the scatter from the planform sheet in the spanwise images is nearly eliminated and vice versa. For the simultaneous image pairs which follow, a white dashed line is used to show the intersection of the two sheets.

Efforts at simultaneously imaging the streamwise and spanwise image planes were much less successful. Since the streamwise sheet must contact the model, simply rotating the polarization of the incoming laser light is no longer effective. The efficiency of the iodine filter was not high enough to absorb all of the stray scatter from the model, and therefore signal to noise ratios remained too low to produce useful image data.

3. Results

Single-shot FRS images of the centerline boundary layer taken with both streamwise and spanwise laser sheet orientations are presented. The individual frames illustrate the structures present as the boundary layer undergoes transition. Stability analysis [3] has predicted that transition would occur in the regions off-axis where the crossflow velocities are highest. Instead, recent experiments [5] have found that the first evidence of transition occurs in the centerline region, where the symmetry requires that the crossflow velocity is zero. The spanwise images reveal the mechanism by which the centerline boundary layer breaks down. This process is shown here for the first time.

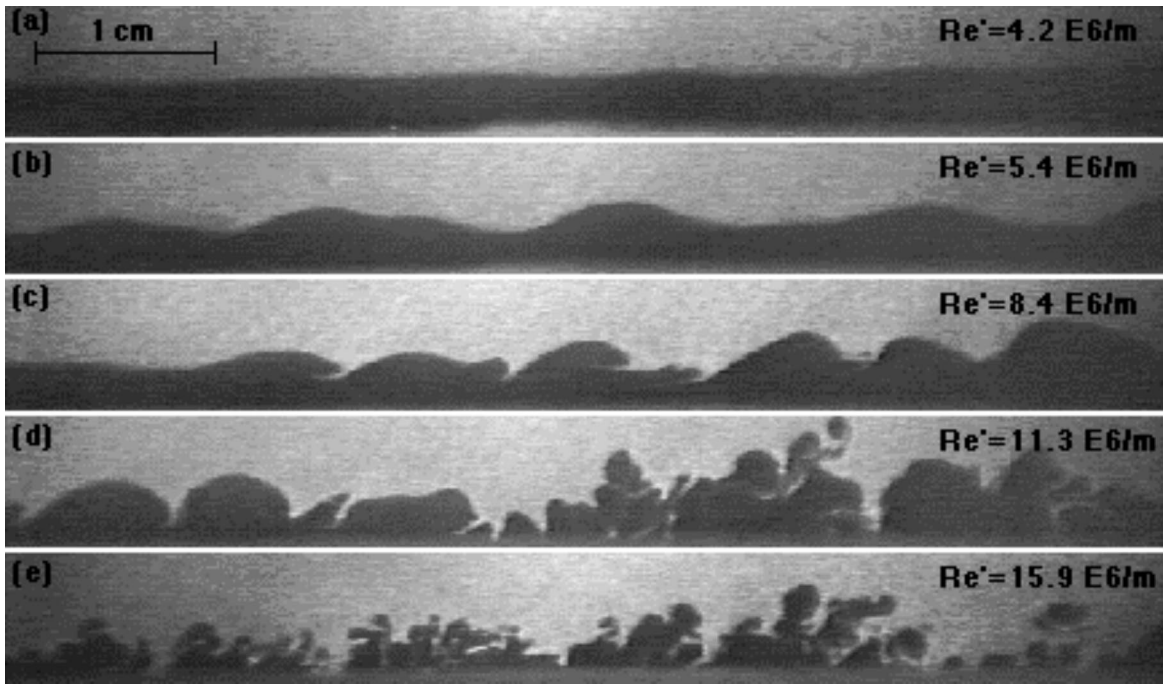

Figure 4. Streamwise Filtered Rayleigh Scattering on 4 : 1 Elliptic Cone. Flow is left to right. The center of each frame is approximately 21 cm from the nose of the model. The model surface coincides with the bottom line of each frame.

Simultaneous images of planform and spanwise slices through the boundary layer are also presented. Images taken at various heights throughout the boundary layer show the spanwise extent and shape of the structures which appear in the early stages of transition.

3.1. Streamwise images

Figure 4 is a montage of images taken at the same streamwise position along the 4 : 1 cone for five different unit Reynolds numbers. Each image is meant to be a representative sample of the boundary layer behavior at that particular value of Re_x. The character ranges from what appears to be fully laminar in frame *4*(*a*) to late-transitional in frames *4*(*d*) and *4*(*e*). All of the images were taken with a moderate cold wall condition ($\mathrm{Tw}/\mathrm{To} = 0.53 \pm 0.03$) with a streamwise field of view ranging from 19 to 25 cm from the nose of the model. Pitot surveys of the centerline boundary layer have shown that the visualized interface between condensed (light) and sublimated (dark) CO_2 occurs at approximately 0.9δ. Frame *4*(*b*), taken at $\mathrm{Re}' = 5.4 \times 10^6/\mathrm{m}$, contains a traveling wave with a wavelength between four and five times the boundary layer thickness. Higher frequency traveling waves appear in frame *4*(*c*). At this higher Reynolds number, the wavelength decreases to delta approximately twice the boundary layer thickness. Since the visualization technique is sensitive to temperature, the observed waves represents density fluctuations. Using hot-wire anemometry on a 7 degree axisymmetric cone at Mach 8, Stetson et al. [9] determined that high Mach number instabilities produce large density fluctuations and relatively small fluctuations in velocity. The second mode instabilites were highly 'tuned' to the boundary layer thickness, and possessed a wavelength of two times the boundary layer thickness. It was also estimated that another peak frequency (believed to be the first harmonic of the second mode) would correspond to a wavelength approximately equal to the boundary layer thickness.

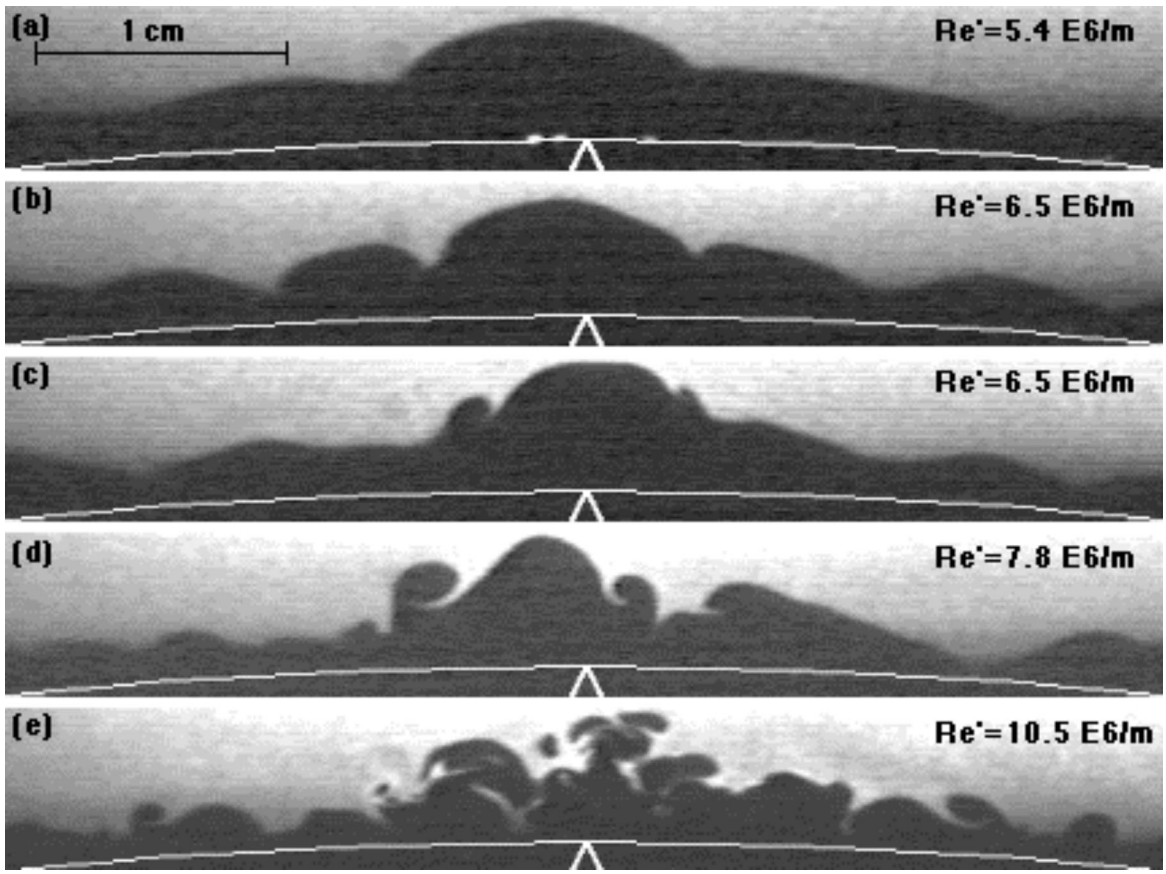

Figure 5. Spanwise Filtered Rayleigh Scattering on 4:1 Elliptic Cone. Flow is out of the plane of the paper. Laser sheet is positioned 21 cm from the nose of model. The cone centerline is marked by the arrow in the bottom of the image.

Frame *4*(*c*) still possesses some traveling wave character, but the interface is becoming highly distorted. As the unit Reynolds number is increased further, frame *4*(*d*) shows the emergence of small-scale bulges forming on the edges of the larger scales. The final frame, taken at $\mathrm{Re}' = 15.9 \times 10^6$, shows almost no evidence of the previous traveling wave structures, and clearly exhibits the small scales characteristic of a turbulent boundary layer.

Overall, from streamwise images taken on centerline, the 4:1 model appears to exhibit transition behavior which is characteristic of two-dimensional or axisymmetric configurations.

3.2. Spanwise images

Figure 5 is a montage of single-shot FRS images which were all taken at the same position (21.0 cm from the nose) along the cone while varying the unit Reynolds number. Each frame is meant to show representative behavior of the boundary layer at that particular Reynolds number. In these images the flow is moving out of the page, and the white arrow at the bottom of each image represents the position of the centerline (minor axis) of the cone. Over the range of Re_x from 1.1×10^6 to 2.2×10^6, these images present a much more complex picture of the dynamics of boundary layer transition than that which was observed in the streamwise images.

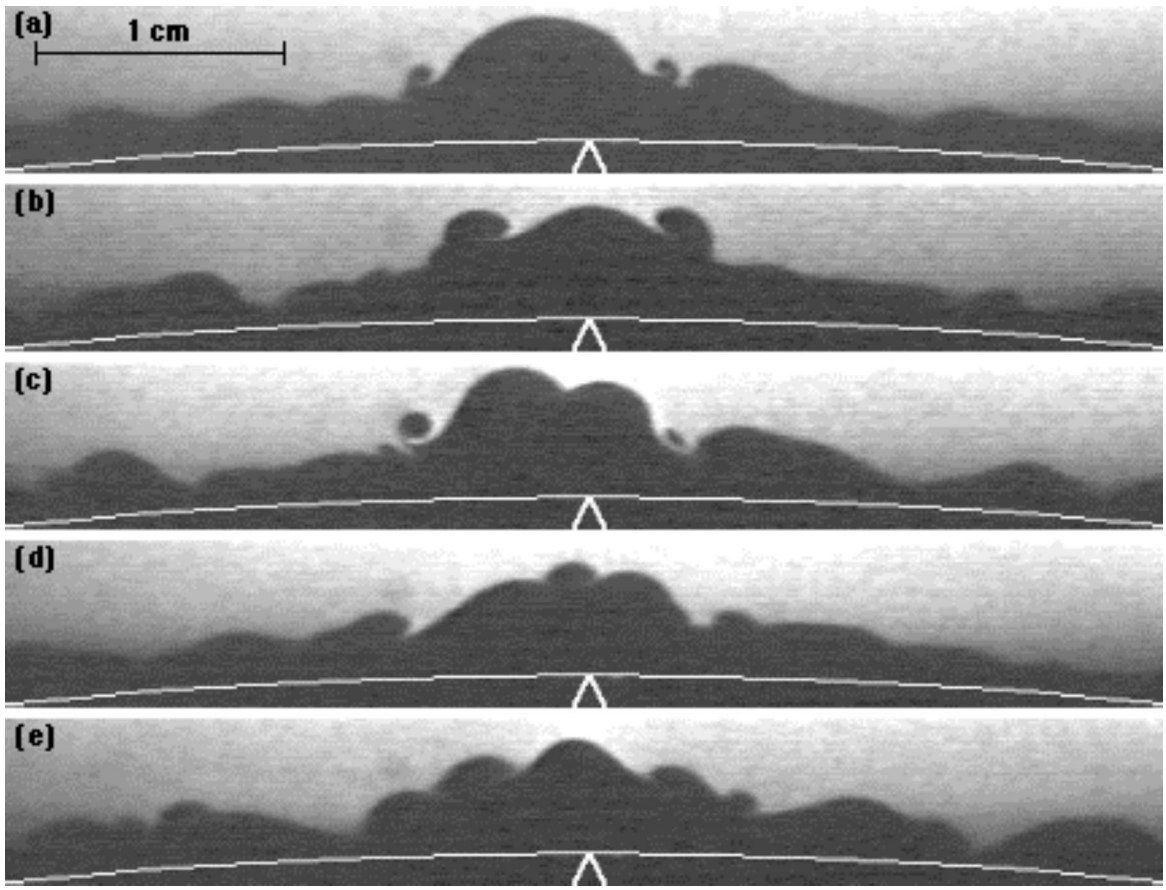

Figure 6. Single-shot spanwise images on 4:1 cone showing the emergence of small-scale vortices. Laser sheet is positioned 21 cm from nose. All images are taken at $\mathrm{Re}' = 7.8 \times 10^6$.

The bulge in the boundary layer near the centerline in *figure 5*(*a*) is a result of the influx of low-momentum fluid from the high-pressure leading edge to the low-pressure centerline of the model. Computations of the laminar flowfield on elliptic cones have also shown the existence of this centerline bulge [3,10,11].

Frames *5*(*b*) and *5*(*c*) were taken at $\mathrm{Re}_x = 1.4 \times 10^6$. The equivalent streamwise images (frame *4*(*b*)) show the beginnings of large traveling waves aligned with the flow. *Figure 5*(*b*) shows wave-like structures which have developed on either side of centerline in the spanwise plane perpendicular to the flow. In spanwise images *5*(*c*) and *5*(*d*) there is also evidence of much smaller scale structures which develop in the regions slightly off the cone centerline. At higher Reynolds numbers, the off-centerline structures can become larger, seemingly wrapping up and growing at the expense of the low-momentum fluid which makes up the centerline bulge.

From these single-shot images, it is clear that the observed small-scale structures possess a vortical character. From the entrainment of condensed CO_2 from the freestream in *figure 5*(*d*), it is possible to conclude that the direction of rotation of these spanwise vortices. With the flow direction out of the page, the small-scale vortical structure to the right of centerline is ‘rolling up’ with streamwise vorticity oriented downstream. Conversely, the structures to the left of centerline possess vorticity oriented upstream.

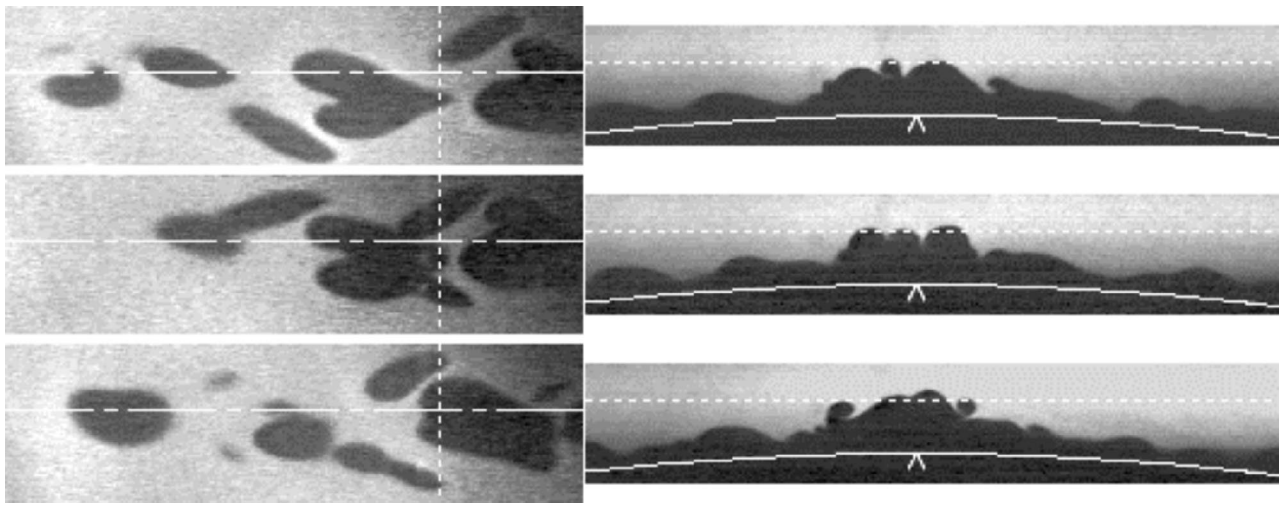

Figure 7. Simultaneous images of planform (left) and spanwise (right) planes. Dashed line represents the intersection of the two planes. Flow is from left to right in planform image and out of the paper plane for the spanwise image. Planform sheet is positioned 4.0 mm from the model surface.

Figure 6 is a montage of single shot images taken at the same Reynolds number. The images illustrate the great variety of distortions that the centerline bulge undergoes as it breaks down. What was once a single bulge, seemingly bifurcates into two (*6*(*c*)) or even three (*6*(*d*)) smaller bulges. The significance of this behavior will become more evident when the planform images are considered. All of the images show evidence of small-scale structures which possess streamwise vorticity. Even though the size of the structure varies, the inferred vorticity is always directed downstream for the structures which develop to the right of centerline.

Unlike some other visualization techniques which suffer from path integration limitations (e.g. schlieren and shadowgraph), the Filtered Rayleigh Scattering technique allowed us to illuminate a thin cross-section of the boundary layer over the elliptic cone. The images appear to capture a purely three-dimensional transition mechanism. The bulge in the boundary layer (which results from mass flux to the centerline induced by spanwise pressure gradients) starts to break down by first developing small-scale vortical structures on either or both sides. The structures evolve and eventually lead to further non-linear processes. In *figure 5*(*e*), the centerline bulge has broken down into smaller scales typical of a late-transitional boundary layer while the regions farther off centerline still appear to be in the early stages of transition. Although on a much smaller scale, the same process seems to be occurring on the spanwise bulges which have developed at a distance 1.5 cm from the centerline on both sides. Near the left and right edges of *figure 5*(*e*), there are small-scale vortical structures which are ‘attached’ to smaller spanwise bulges and appear to possess the same direction of streamwise vorticity seen in the lower Reynolds number images.

3.3. Simultaneous imaging

Figure 7 is a montage of three pairs of simultaneous images taken of the boundary layer in the early stages of transition. The dashed line in the planform images represents the position of the spanwise sheet, while the dashed line in the spanwise image represents the position of the planform sheet. For this series, the planform sheet is placed at a distance 4 mm from the centerline surface of the model. The most striking feature in frames *7*(*a*) and *7*(*b*) is the appearance of a heart-shaped structure in the planform images. In looking at the corresponding spanwise images, it is clear that the middle bulge is actually the tail end of the heart-shaped

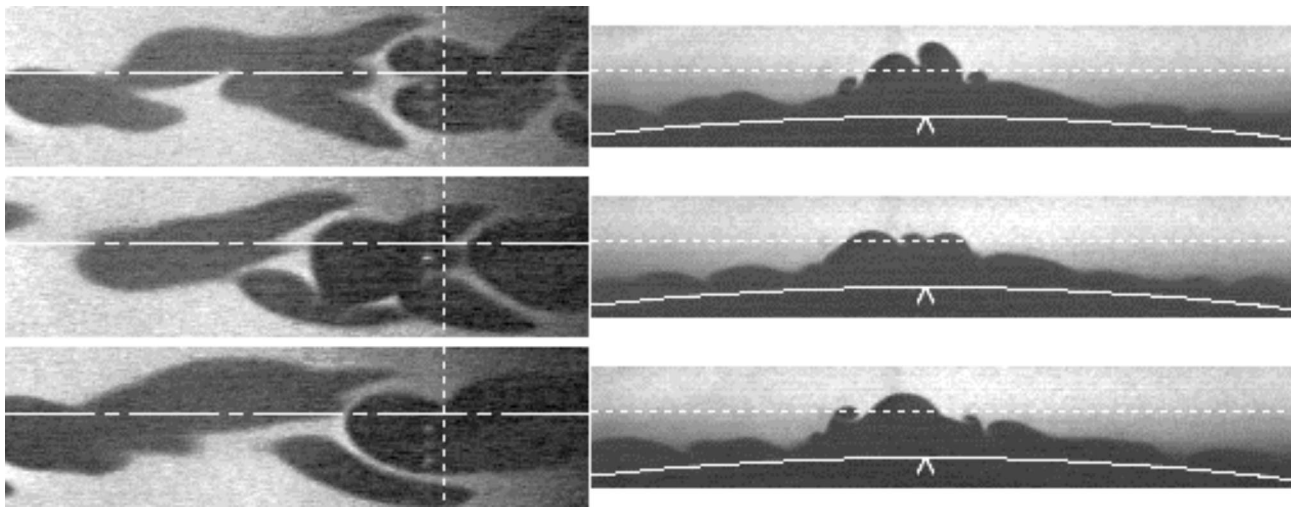

Figure 8. Simultaneous images of planform (left) and spanwise (right) planes. Dashed line represents the intersection of the two planes. Flow is from left to right in planform image and out of the paper plane for the spanwise image. Planform sheet is positioned 3.5 mm from the model surface.

structure. The two 'side bulges' show up in the planform view as long thin structures which are aligned at almost 45 degrees from the flow axis.

In frame *7*(*c*), the spanwise sheet cuts through the front end of the distorted heart-shaped structure. The spanwise image shows that the centerline bulge seems to have broken into two large bulges. The small scale vortical structures which are attached to this 'double-bulge' in the spanwise image again show up as elongated structures in the planform image which are aligned roughly 45 degrees to the flow axis.

These images help to illuminate the behavior observed in the spanwise images shown in *figure 6*. From the planform images, it appears that the centerline bulge is actually highly three-dimensional. When sliced through the upstream edge, images similar to *figure 6*(*c*) are produced. When the spanwise sheet cuts through the middle of the heart, images similar to *6*(*a*) or *6*(*b*) are produced where a single bulge is present with smaller scales developing off-axis. Finally, when images are taken of the downstream edge of the planform heart, the smaller scales have grown to sizes which are equivalent to the original centerline bulge, and it appears as though three bulges exist (*figures 6*(*d*), *7*(*a*), *7*(*b*)).

The images in *figures 8* and *9* are taken with the planform sheet positioned 3.5 and 3.0 mm from the surface, respectively. Again, image pairs have been chosen which capture the different stages of the planform heart-shaped structures. For the planform images taken towards the interior of the boundary layer, the extent of the small vortical structures is shown. From *figure 9*(*a*), it is apparent that the small-scale structures imaged in the spanwise view actually extend far upstream. In fact, what appeared to be two separate structures may be one continuous loop which wraps around the upstream edge of the heart-shaped structure.

The planform images are of importance in determining the physical mechanism behind these structures which appear in the early stages of transition. Since our use of the Filtered Rayleigh Scattering technique depends on condensed CO_2 to enhance the signal, it is possible to make assumptions about the flow direction in the planform images. The bright regions of condensed CO_2 are assumed to possess downward velocity, since this would represent freestream fluid which is being entrained in the boundary layer but which has not yet been close enough to the wall to sublimate the CO_2. Conversely, the dark regions represent fluid that has already come in close contact with the wall, and is now moving away from the surface.

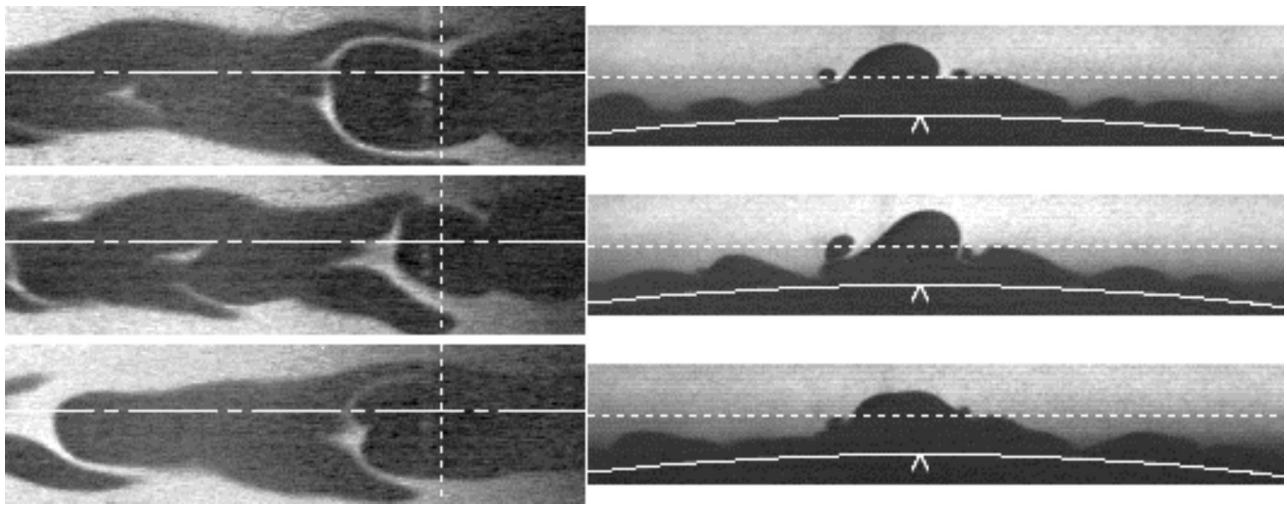

Figure 9. Simultaneous images of planform (left) and spanwise (right) planes. Dashed line represents the intersection of the two planes. Flow is from left to right in planform image and out of the paper plane for the spanwise image. Planform sheet is positioned 3.0 mm from the model surface.

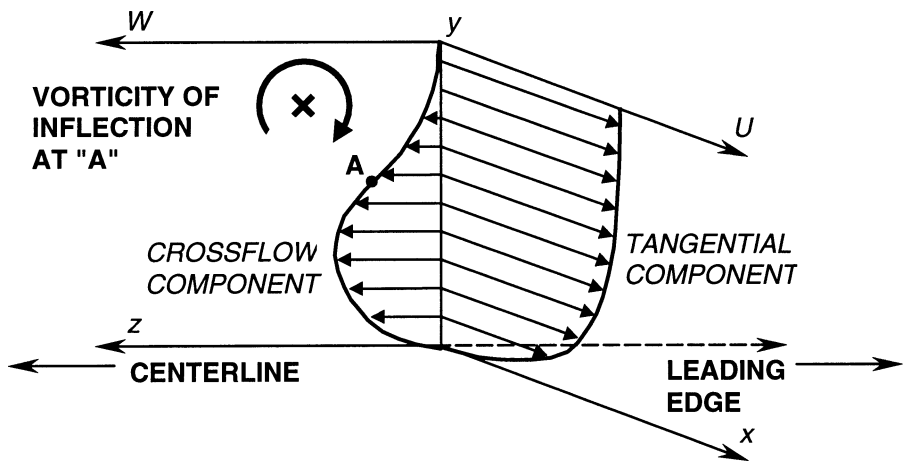

Figure 10. Diagram of inflectional crossflow velocity profile in the off-axis region to the right of centerline. Associated vorticity is oriented upstream.

4. Conclusions

Streamwise visualizations have shown the existence of traveling wave instabilities on the centerline of the elliptic cone. Wavelengths indicate that the disturbances may be associated with the second mode instabilities characteristic of two-dimensional and axisymmetric configurations.

Spanwise visualization of the boundary layer showed small-scale structures which were not apparent in the streamwise direction. Previous computational research (Huang et al. [3]) has indicated that the inflectional crossflow velocity profile could lead to an inviscid instability and early transition on elliptic cone geometries. In our spanwise views, this proposed inviscid instability should appear far off centerline in the region of maximum crossflow. The inflectional instability should grow as a Kelvin–Helmholtz-type roll-up with a component of vorticity oriented upstream for flow on the starboard side of the cone. *Figure 10* illustrates this concept.

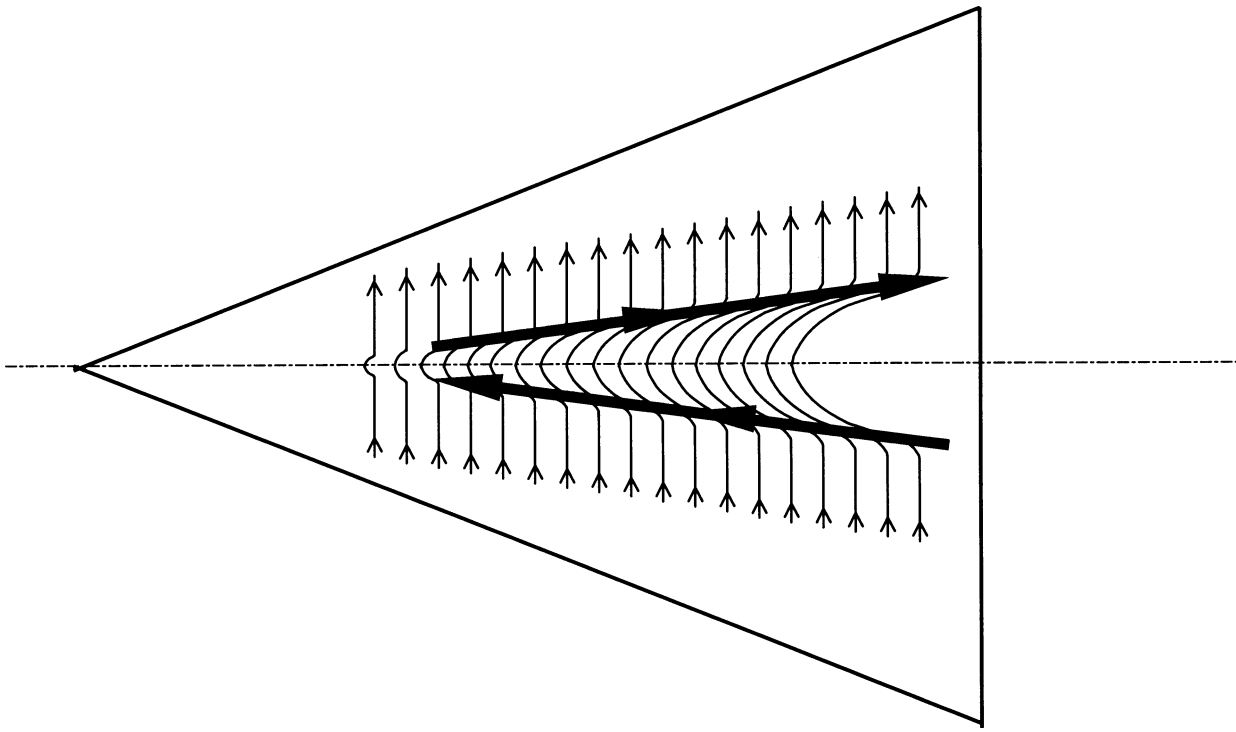

Figure 11. Diagram showing distortion of boundary layer vortex sheet due to presence of centerline bulge. The bold lines represents the resulting components of streamwise vorticity which match the direction observed in the spanwise visualizations.

From the flow visualizations presented in this paper, evidence of transition begins close to the centerline and not in the regions of maximum crossflow. The process begins with the emergence of streamwise vortices on either side of the centerline bulge. The orientation of the vorticity vector is downstream for the structure appearing to the right of centerline. This suggests a mechanism which would require a crossflow profile with an inflection of the opposite sense to that shown in *figure 10*. Certainly, the instability mechanism is not directly associated with the predicted crossflow instability. In light of this finding, the linearized assumption made in the numerical results may not accurately predict transition in flow fields with a high degree of three-dimensionality.

The mechanism by which streamwise vorticity is produced involves the stretching and tilting of vortex lines which originate in the boundary layer. *Figure 11* illustrates how the streamwise components of vorticity could be strengthened by the distortion of the vortex lines due to the low-momentum bulge which forms on the centerline. In the presence of the growing bulge, the vortex lines on the centerline may lag behind the sections which are farther off-axis. Tilting of the line to accommodate the slower-moving centerline sections could occur, and the streamwise component of vorticity will then increase. The final result is a flow field over the top of the cone which includes large concentrations of streamwise vorticity positioned on either side of the centerline axis. The vortex tube to the right of centerline is oriented downstream, while the adjacent tube possesses vorticity oriented upstream.

The vorticity associated with the crossflow velocity profile is not responsible for the structures observed in the spanwise visualizations. The main role of the crossflow appears to be a mechanism which causes a spanwise mass flux component, directed to the centerline. This mass flux gathers along the axis of symmetry and causes a bulge in the centerline velocity profile which distorts the spanwise vorticity in the boundary layer. The resulting streamwise components of vorticity match the position and direction of the vortical structures observed in the

spanwise visualizations. The final breakdown of the boundary layer observed in the streamwise visualizations still appears qualitatively similar to that which occurs on axisymmetric configurations [9].

Questions still remain as to the role of the traveling waves seen in the streamwise visualizations and how they effect the behavior of the spanwise mechanisms. Future work on this model will include the imaging of consecutive frames to analyze the development of structures seen in these single-shot images.

Acknowledgments

The support from AFOSR grant F49620-97-1-0181 is gratefully acknowledged.

References

[1] Mack L.M., Boundary-layer stability theory, Special course on stability and transition of laminar flow, AGARD Report 709, 1984.
[2] Stetson K.F., Kimmel R.L., On hypersonic boundary-layer stability, AIAA Paper 92-0737, 1992.
[3] Huang S.L., Stuckert G.K., Herbert T., Crossflow instability of the supersonic flow over a 4 : 1 elliptic cone, AFOSR Report F49620-94-C-0053, 1995.
[4] Stetson K.F., Thompson E.R., Donaldson J.C., Siler L.G., Laminar boundary-layer stability experiments on a cone at Mach 8, part 3: sharp cone at angle of attack, AIAA Paper 85-0492, 1985.
[5] Poggie J., Kimmel R.L., Traveling instabilities in elliptic cone boundary-layer transition at Mach 8, AIAA Paper 98-0435, 1998.
[6] Baumgartner M.L., Turbulence structure in a hypersonic boundary layer, Ph.D. Thesis, Princeton University, 1997.
[7] Erbland P.J., Baumgartner M.L., Yalin A.P., Etz M.R., Muzas B., Lempert W.R., Smits A.J., Miles R.B., Development of planar diagnostics for imaging Mach 8 flowfields using carbon dioxide and sodium seeding, AIAA Paper 97-0154, 1997.
[8] Poggie J., Smits A.J., Quantitative visualization of supersonic flow using Rayleigh scattering, AIAA Paper 96-0436, 1996.
[9] Stetson K.F., Thompson E.R., Donaldson J.C., Siler L.G., Laminar boundary layer stability experiments on a cone at Mach 8, part 1: sharp cone, AIAA Paper 83-1761, 1983.
[10] Kimmel R.L., Schwoerke S.N., Klein M.A., Three-dimensional hypersonic laminar boundary layer computations for transition experiment design, AIAA Paper 96-2080, 1996.
[11] Lyttle I.J., Reed H.S., Use of transition correlations for three-dimensional boundary layers within hypersonic flows, AIAA Paper 95-2293, 1995.